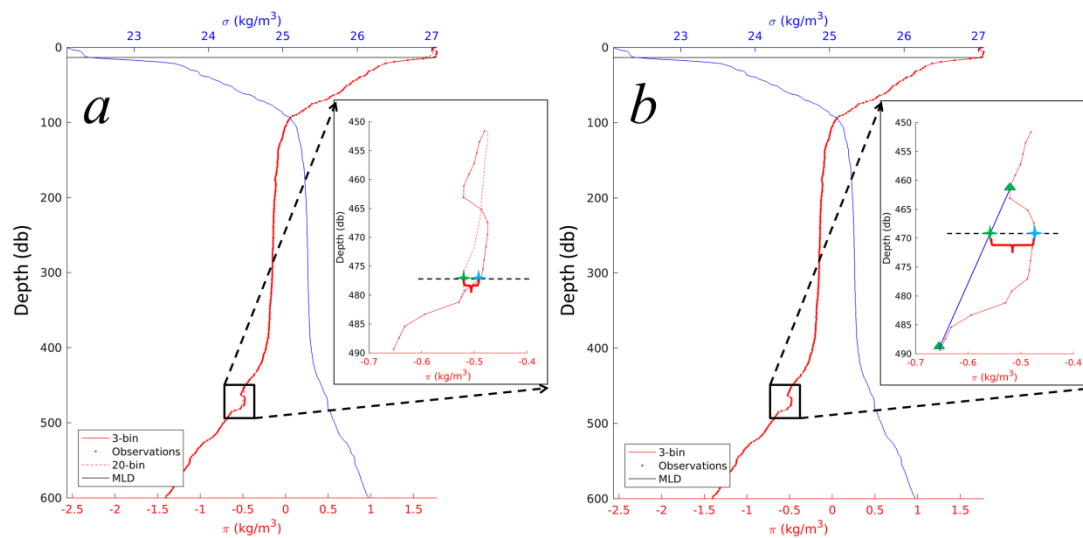


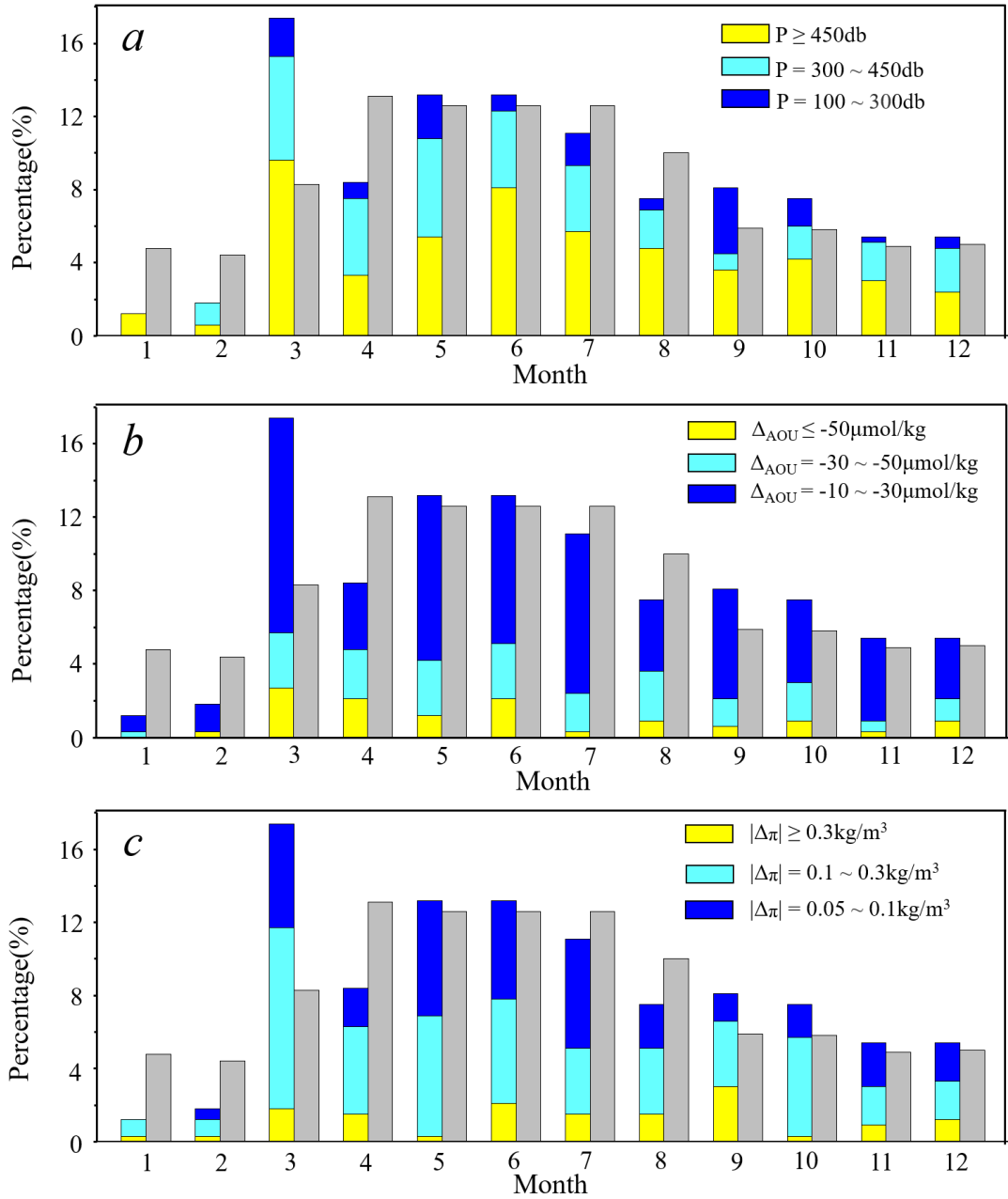
1 Supplemental file

2



3

4 **Fig. S1** A case profile (profile No. 136 of float MR2901556, box 2 in Fig. 2) with  
5 apparent subduction signals in  $\pi$  anomalies to illustrate the validity of our algorithm  
6 (see Methods) but the failure of the method by Llort et al. (2018) in identifying the  
7 visible subduction signal. The derived  $\pi$  anomaly based on 20-bin running averages is  
8 significantly dampened and too small ( $0.03 \text{ kg/m}^3$ , inset in panel a) to exceed the  
9 defined threshold ( $0.05 \text{ kg/m}^3$ ); yet the  $\pi$  anomaly identified from our approach is  
10 much larger ( $0.07 \text{ kg/m}^3$ , inset in panel b). The potential density and potential spicity  
11 were referenced to surface pressure.



12

13 **Fig. S2** Statistics of the subduction patches detected in each month, accumulated in  
 14 terms of different intervals of subduction depths (a) and strengths (b and c). The grey  
 15 bars in each panel represent the percentage of the number of profiles available in each  
 16 month.

17

18 **Table S1** Sensitivity of the newly-modified algorithm to the interval of  $\Delta\rho$  by varying  
 19 it between 70db and 130db, with statistics of how many more/less patches were  
 20 detected, and the root mean square difference (RMSD) of the integrated  $\Delta_{\text{AOU}}$  and  
 21 total  $\Delta\pi$  between the new  $\Delta\rho$  and  $\Delta\rho$  of 100db. The row marked in red refers to the  $\Delta\rho$   
 22 used in this study and the total number of subduction patches identified.

$\Delta p$ (db)	Total patches	$\pm\%$ in total N	RMSD of $\sum\Delta_{\text{AOU}}$ ( $\mu\text{mol/kg}$ )	RMSD of $\sum\Delta_{\pi}$ ( $\text{kg/m}^3$ )
$\Delta p=130$	326	-2.7%	8.9(17.7%)	0.04(16.8%)
$\Delta p=120$	329	-1.8%	6.7(18.4%)	0.04(15.9%)
$\Delta p=110$	330	-1.5%	5.1(10.8%)	0.03(11.5%)
$\Delta p=105$	329	-1.8%	4.0(6.9%)	0.03(7.3%)
$\Delta p=103$	332	-1.0%	3.8(6.6%)	0.02(6.9%)
$\Delta p=102$	334	-0.0%	3.7(5.5%)	0.01(4.5%)
$\Delta p=101$	335	0.0%	3.4(4.3%)	0.01(4.2%)
<b><math>\Delta p=100</math></b>	<b>335</b>	<b>0</b>	<b>0</b>	<b>0</b>
$\Delta p=99$	330	-1.5%	3.3(7.9%)	0.03(8.8%)
$\Delta p=98$	328	-2.0%	3.5(8.2%)	0.03(9.1%)
$\Delta p=97$	328	-2.0%	3.6(8.3%)	0.03(9.2%)
$\Delta p=95$	326	-2.7%	4.0(9.4%)	0.03(9.7%)
$\Delta p=90$	317	-5.4%	6.2(11.8%)	0.04(12.8%)
$\Delta p=80$	306	-8.7%	10.6(18.9%)	0.08 (16.4%)
$\Delta p=70$	284	-15.2%	15.6(23.4%)	0.1(22.4%)

23

24 **Table S2** Statistics of the subduction patches identified in each depth interval, and the  
25 associated anomalies in AOU, DO and  $\pi$  on average.

Depth interval (db)	Number of subduction	Mean $\Delta_{\text{AOU}}$ ( $\mu\text{mol/kg}$ )	Mean $\Delta_{\text{DO}}$ ( $\mu\text{mol/kg}$ )	Mean $\Delta_{\pi}$ ( $\text{kg/m}^3$ )
100-200	8 (2.25%)	-20.89 $\pm$ 6.20	30.77 $\pm$ 12.39	0.33 $\pm$ 0.12
200-300	41 (11.55%)	-28.80 $\pm$ 16.55	34.87 $\pm$ 20.84	0.13 $\pm$ 0.09
300-400	87 (24.51%)	-30.34 $\pm$ 16.55	37.64 $\pm$ 18.70	0.18 $\pm$ 0.12
400-500	69 (19.44%)	-29.30 $\pm$ 17.08	35.46 $\pm$ 21.05	0.18 $\pm$ 0.13
500-600	57 (16.06%)	-28.94 $\pm$ 17.37	37.76 $\pm$ 22.17	0.20 $\pm$ 0.15
600-700	60 (16.90%)	-22.92 $\pm$ 12.74	29.37 $\pm$ 16.80	0.15 $\pm$ 0.11
700-800	13 (3.66%)	-16.50 $\pm$ 8.20	19.16 $\pm$ 13.61	0.18 $\pm$ 0.12

26

### 27 **Text S1: Sensitivity analysis**

28 To investigate the robustness and representativeness of the results derived using the  
29 newly-modified algorithm (see Methods), we examined the sensitivity of the  
30 algorithm to the interval of  $\Delta p$  by varying it between 70db and 130db. In each test of  
31  $\Delta p$  (i.e., 70db, 80db, 90db, 95db, 97db, 98db, 99db, 101db, 102db, 103db, 105db,  
32 110db, 120db, and 130db), the total number of subduction patches identified and the

33 corresponding strengths of  $\Delta_{\text{AOU}}$  and  $\Delta_{\pi}$  integrated for each Julian day were quantified,  
34 and these statistics were compared with those based on  $\Delta p$  of 100m (following Fig. 4).  
35 Statistical measures include how many more/less patches were detected, and the  
36 RMSD of the integrated  $\Delta_{\text{AOU}}$  and total  $\Delta_{\pi}$  between the new  $\Delta p$  and  $\Delta p$  of 100m  
37 (Table S1).

38 In general, our choice of  $\Delta p$  of 100 db is reasonable and should be the most  
39 representative based on the statistics in Table S2. In each test using a new  $\Delta p$ , a few  
40 subudction patches failed to be identified. Specifically, for  $\Delta p$  of  $100 \pm 3$ db (i.e., 97db,  
41 98db, 99db, 101db, 102db, and 103db), less than 7 ( $\leq 2\%$ ) subduction patches were  
42 missed, and the resulted  $\Delta_{\text{AOU}}$  and  $\Delta_{\pi}$  show a RMSD of  $\leq 3.8 \mu\text{mol/kg}$  ( $\leq 8.3\%$ ) and  $\leq$   
43  $0.03 \text{ kg/m}^3$  ( $\leq 9.2\%$ ). For  $\Delta p \leq 95$ db and  $\Delta p \geq 105$  db, the number of missed  
44 subduction patches were even bigger, with a maximum number of missing patches of  
45 51 (15.2%) in case of  $\Delta p=70$ db. It should be noted that, although the  $\Delta p$  was varied at  
46 a fine vertical resolution (i.e., 1db, 5db, 10db), the vertical sampling frequency of the  
47 BGC-Argo floats changes with depth ((i.e., every 5db, 10db, and 50db for depth  
48 intervals of 0-100db, 100-500db, and 500-1000db, respectively). This coarse sampling  
49 particularly at depth is mainly responsible for the resulted changes in  $\Delta_{\text{AOU}}$  and  $\Delta_{\pi}$ .